The Astrophysical Journal, 799:123 (10pp), 2015 February 1 doi:10.1088/0004-637X/799/2/123

NuSTAR OBSERVATION OF A TYPE I X-RAY BURST FROM GRS 1741.9-2853

Nicolas M. Barrière[1], Roman Krivonos[1], John A. Tomsick[1], Matteo Bachetti[2], Steven E. Boggs[1], Deepto Chakrabarty[3], Finn E. Christensen[4], William W. Craig[1,5], Charles J. Hailey[6], Fiona A. Harrison[7], Jaesub Hong[8], Kaya Mori[6], Daniel Stern[9], and William W. Zhang[10]
[1] Space Sciences Laboratory, University of California, Berkeley, CA 94720, USA; barriere@ssl.berkeley.edu
[2] Institut de Recherche en Astrophysique et Plantologie, UMR 5277, Toulouse, France
[3] MIT Kavli Institute for Astrophysics and Space Research, Massachusetts Institute of Technology, Cambridge, MA 02139, USA
[4] National Space Institute, Technical University of Denmark, Copenhagen, Denmark
[5] Lawrence Livermore National Laboratory, Livermore, CA 94550, USA
[6] Columbia Astrophysics Laboratory, Columbia University, New York, NY 10027, USA
[7] Cahill Center for Astronomy and Astrophysics, Caltech, Pasadena, CA 91125, USA
[8] Harvard-Smithsonian Center for Astrophysics, Cambridge, MA 02138, USA
[9] Jet Propulsion Laboratory, California Institute of Technology, Pasadena, CA 91109, USA
[10] X-ray Astrophysics Laboratory, NASA Goddard Space Flight Center, Greenbelt, MD 20771, USA
Received 2014 May 20; accepted 2014 November 21; published 2015 January 21

ABSTRACT

We report on two *NuSTAR* observations of GRS 1741.9-2853, a faint neutron star (NS) low-mass X-ray binary burster located 10′ away from the Galactic center. *NuSTAR* detected the source serendipitously as it was emerging from quiescence: its luminosity was 6×10^{34} erg s^{-1} on 2013 July 31 and 5×10^{35} erg s^{-1} in a second observation on 2013 August 3. A bright, 800 s long, H-triggered mixed H/He thermonuclear Type I burst with mild photospheric radius expansion (PRE) was present during the second observation. Assuming that the luminosity during the PRE was at the Eddington level, an H mass fraction $X = 0.7$ in the atmosphere, and an NS mass $M = 1.4\,M_{\odot}$, we determine a new lower limit on the distance for this source of 6.3 ± 0.5 kpc. Combining with previous upper limits, this places GRS 1741.9-2853 at a distance of 7 kpc. Energy independent (achromatic) variability is observed during the cooling of the NS, which could result from the disturbance of the inner accretion disk by the burst. The large dynamic range of this burst reveals a long power-law decay tail. We also detect, at a 95.6% confidence level (1.7σ), a narrow absorption line at 5.46 ± 0.10 keV during the PRE phase of the burst, reminiscent of the detection by Waki et al. We propose that the line, if real, is formed in the wind above the photosphere of the NS by a resonant Kα transition from H-like Cr gravitationally redshifted by a factor $1 + z = 1.09$, corresponding to a radius range of 29.0–41.4 km for a mass range of 1.4–2.0 $M_{\odot}$.

Key words: accretion, accretion disks – nuclear reactions, nucleosynthesis, abundances – stars: neutron – X-rays: binaries – X-rays: bursts – X-rays: individual (GRS 1741.9-2853)

1. INTRODUCTION

GRS 1741.9-2853 (also called AX J1745.0-2855) is a very faint X-ray transient that was discovered by the *Granat* satellite in 1990 (Sunyaev 1990). In 1996, *Beppo-SAX* detected a series of three Type I bursts from this source, establishing that it is a neutron star (NS) low-mass X-ray binary (LMXB; Cocchi et al. 1999). Since its discovery, GRS 1741.9-2853 has been detected in outburst several times by different observatories; in 1994, 1996, 2000, 2002, 2005, 2007, 2009, 2010, and in 2013 (Sakano et al. 2002; Muno et al. 2003, 2007; Wijnands et al. 2005, 2006, 2007; Porquet et al. 2007; Chenevez et al. 2009; Trap et al. 2009; Kennea 2009; Degenaar et al. 2010, 2013b; Degenaar & Wijnands 2010; Kuulkers et al. 2013). Its typical outburst luminosity is $\sim 10^{35-36}$ erg s^{-1} (see Trap et al. 2009; Degenaar et al. 2014 for reviews of GRS 1741.9-2853 earlier and more recent outburst history). It has also been detected in quiescence by *Chandra*, with a 2–8 keV luminosity of about 10^{32} erg s^{-1} (Muno et al. 2003). Its outburst duty cycle is about 10%, with typical outburst duration of $\sim$10 weeks and recurrence time of $\sim$2 years. Its average accretion rate in outburst is of the order of $10^{-10}\,M_{\odot}$ yr^{-1} (Degenaar & Wijnands 2010). A distance measurement of 8 kpc was proposed by Cocchi et al. (1999), placing the source very close to the Galactic center, as it lies 10′ from Sagittarius A*. This distance was then further refined to an upper limit of 7 kpc by Trap et al. (2009), who used *INTEGRAL*, *XMM-Newton*, and *Swift* data of the 2005 and 2007 outbursts.

GRS 1741.9-2853 is a binary system where the companion is a low-mass star ($M \leqslant 1\,M_{\odot}$) filling its Roche lobe and pouring matter onto an accretion disk. The known LMXBs in our Galaxy are concentrated in the Galactic bulge (Grimm et al. 2002; Revnivtsev et al. 2008), and half of them are transients that increase their luminosity by several orders of magnitudes during outbursts (Liu et al. 2007). In such systems, X-ray outbursts are interpreted as an increase of the accretion rate onto the compact object (e.g., Osaki 1974). In the category of the *very faint* transients (2–10 keV luminosity in the 10^{34-36} erg s^{-1} range during outburst), which includes GRS 1741.9-2853, the alternation between quiescence and outburst can be described by the thermal-viscous disk instability model, where the disk spends most of its time in a cold neutral phase (quiescence), and sometimes becomes hot and ionized, triggering accretion and causing an outburst (see Lasota 2001 for a review). The source then goes back to quiescence, allowing the disk to refill until the cycle starts again. The very faint transients are not well studied, and in particular, the evolutionary scenario that leads to these very low time-averaged accretion rate systems is not clear (King & Wijnands 2006).

In many NS LMXBs, outbursts are punctuated by Type I X-ray bursts, which appear as a sudden increase of luminosity

(by up to two orders of magnitude) followed by an exponential or power-law decay with a duration ranging from a few seconds to several hundreds of seconds, and even up to a few tens of hours for the so-called super bursts. These bursts are thermonuclear flashes occurring at the surface of the NS (see Lewin et al. 1993; Strohmayer & Bildsten 2006 for reviews). Their spectrum is well modeled by a blackbody, arising from the hot photosphere of the NS during thermonuclear reactions and decaying during its subsequent cool down. These explosions result from the unstable burning of accreted H and/or He from the companion star. The accreted matter can fuse in different processes depending on its composition and the accretion rate (e.g., Bildsten 1998; Peng et al. 2007).

The observation of a Type I burst from an LMXB securely identifies it as an NS system. In addition, the study of these bursts probes both NS structure and fundamental physics. Their interpretation is rather simple in the first approximation: in the following we assume that the NS emits a pure Planck spectrum isotropically from its entire surface. Under this assumption, in the case a burst is bright enough to lift the photosphere (i.e., a burst with photospheric radius expansion, or PRE burst), the measurement of the luminosity (assumed to be the Eddington luminosity) and temperature can lead to the determination of the distance, and, in theory, of the radius and mass of the NS (Damen et al. 1990), which constrains the equation of state of ultra-dense matter (e.g., Lattimer & Prakash 2001; Özel 2006). Determining the gravitational redshift at the surface of the NS (and thus the mass-to-radius ratio of the NS) can also be done via the observation of spectral features during the burst, either absorption lines (van Paradijs 1979) or absorption edges (in't Zand & Weinberg 2010). This is the most direct method of determining the mass-to-radius ratio, however detections of absorption lines are controversial (Waki et al. 1984; Nakamura et al. 1988; Magnier et al. 1989; Cottam et al. 2002).

In this paper, we report on the detection of a Type I X-ray burst from the faint system GRS 1741.9-2853. In Section 2, we describe the observations in which GRS 1741.9-2853 was detected, as well as the data analysis tools and methods that we used. The outburst and burst light curves are presented in Section 3. The different outburst phases are analyzed in Section 4, and the burst analysis is presented in Section 5. An absorption line was found in the spectrum of the burst; it is described in Section 5.1. In Section 5.2, we searched for a pulsation during the burst and the outburst but found none. Finally, a discussion of these results is presented in Section 6. Uncertainties at the 90% confidence limit are quoted throughout this paper, unless noted.

2. OBSERVATION, DATA REDUCTION, AND DATA ANALYSIS

NuSTAR is a hard X-ray (3–79 keV) focusing telescope with two identical, co-aligned telescopes producing a point spread function of 58″ half power diameter (18″ FWHM). Its effective area peaks at ≈900 cm^2 (adding up the two modules) around 10 keV, and its energy resolution at 10 keV is 400 eV (Harrison et al. 2013).

GRS 1741.9-2853 was detected serendipitously in two tiles of the Galactic survey (Harrison et al. 2013) conducted by *NuSTAR* on 2013 July 31 (obsID 40031001002, 44.4 ks on-time) and on 2013 August 3 (obsID 40031003002, 40.4 ks on-time). The source was brightening during the first observation as it was rising from quiescence (Degenaar et al. 2014). The outburst became more intense and underwent a bright Type I burst during the second observation, starting on 2013 August 3 at UT 23:03:15 (referred to as t_s hereafter).

The data was processed by the *NuSTAR* Data Analysis Software (NuSTARDAS) v1.3.0, which is distributed with HEASOFT v6.15, and uses the calibration files v20131007. Spectra and light curves were extracted using the "nuproducts" FTOOL from the focal plane modules A and B (FPMA and FPMB). Our extraction region is centered on $\alpha_{J2000} = 17^h45^m2\overset{s}{.}47$, $\delta_{J2000} = -28^\circ54'54\overset{''}{.}79$, which is consistent within typical *NuSTAR* astrometric uncertainty ($\leqslant 10''$) to the position reported in Muno et al. (2003). A circular extraction region of 120″ radius was used for the study of the burst, and a 60″ radius was used for the study of the outburst.

We performed the spectral analysis with the Interactive Spectral Interpretation System (ISIS; Houck & Denicola 2000), using Verner et al. (1996) atomic cross sections and Wilms et al. (2000) abundances for the interstellar absorption. We used χ^2 statistics to evaluate the quality of the fit of the different spectral models. We analyzed the data over the range 3–30 keV as both the outburst and the burst spectra cut off sharply above 30 keV. The spectral binning is identical for each spectrum presented in this paper: spectra of FPMA and FPMB were combined, and the spectral bins were grouped to reach at least 50 source + background counts and 3σ signal-to-noise significance in each group. The study of the outburst uses a different region from the same detector chip as background (identical time), and the study of the burst uses the same region as used for source extraction, but taking times preceding the burst as background.

3. LIGHT-CURVE ANALYSIS

The light curves were corrected for dead time (which reaches 45% at the peak of the burst), finite extraction region, and vignetting effects. Figure 1 shows the 3–30 keV light curves of the two observations. The first observation (hereafter referred to as O1) shows a continuous flux rise, revealing the beginning of the outburst (Degenaar et al. 2014). In the second observation (right panel), five periods are distinguished: the "low level" outburst at the beginning of the observation (O2), the rise (O3), the pre-burst (O4), the burst, and post-burst (O5).

Figure 2 shows a close-up view of the burst with finer bins. The burst rise, peak, and early decay is well described by a fast rise exponential decay (FRED) function, with a plateau inserted at the peak:

$$f(t) = \begin{cases} \exp\left(-\frac{\tau_R}{t} - \frac{t}{\tau_D}\right) & 0 < t \leqslant t_{\rm peak} \\ \exp\left(-2\sqrt{\frac{\tau_R}{\tau_D}}\right) & t_{\rm peak} < t \leqslant t_{\rm peak} + t_{\rm plateau} \\ \exp\left(-\frac{\tau_R}{t - t_{\rm plateau}} - \frac{t - t_{\rm plateau}}{\tau_D}\right) & t > t_{\rm peak} + t_{\rm plateau} \end{cases} \quad (1)$$

with $t_{\rm peak} = \sqrt{\tau_R \tau_D}$, the time to reach the peak luminosity, τ_R and τ_D the characteristic rise and decay times, respectively, and $t_{\rm plateau}$ the duration of the plateau. Binning the light curve to 0.5 s bins, the best fit to the data returns a rise time of 4.2 s (time to reach 90% of the peak value), $t_{\rm plateau} = 18$ s, and an e-folding time of 20.6 s (time to decrease by a factor $e^1 \approx 2.72$). The burst lasts over 800 s (*NuSTAR* did not catch the end of the decay because of an Earth occultation), and its decay is unusual with variability between 48 s and 95 s into the burst. The hardness ratio remains constant within errors during these variations, which is similar to the energy-independent (i.e., achromatic) late-time variability observed by in't Zand et al. (2011).

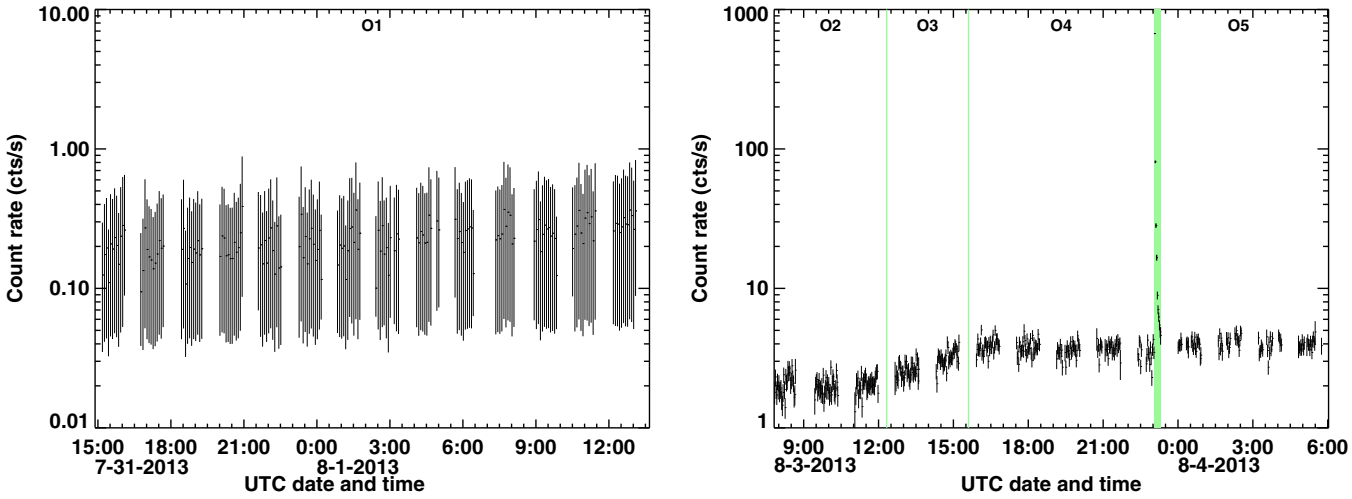

Figure 1. Light curve of GRS 1741.9-2853 during obsIDs 40031001002 (300 s bins, left panel) and 40031003002 (100 s bins, right panel) in the 3–30 keV band. Instrumental background is subtracted and FPMA and FPMB are combined. Error bars show the 1σ uncertainty level. For spectral analysis, the outburst is split into five phases as shown by the green vertical lines and marked by the labels at the top of the plot frames (the first phase, O1, is simply defined as the first observation).

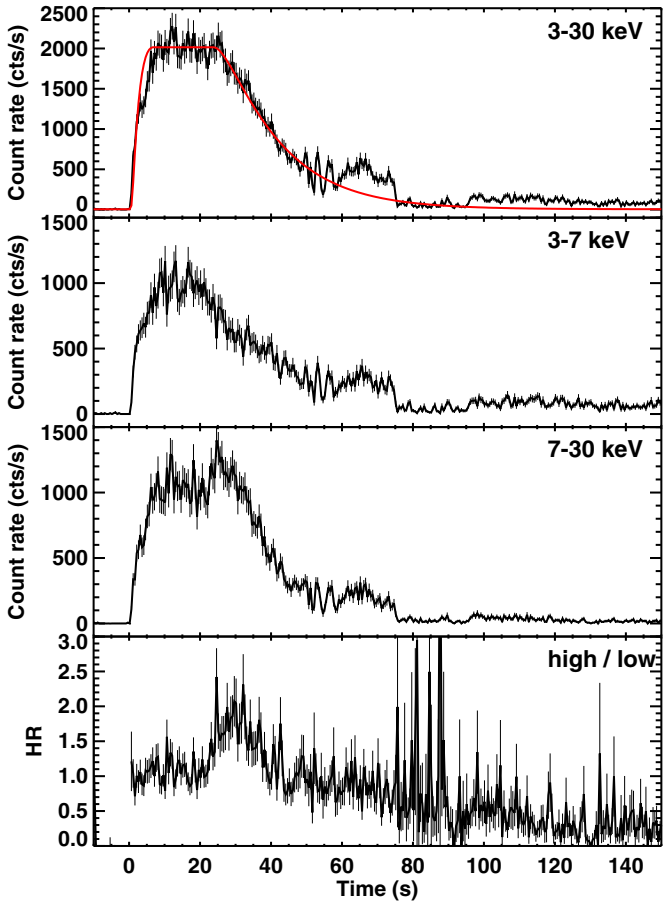

Figure 2. Burst light curve (0.5 s bins) in the 3–30 keV, 3–7 keV, and 7–30 keV bands, and ratio of the 7–30 keV to the 3–30 keV bands. The origin of the time marks the beginning of the burst at 23:03:15 UT on 2013 August 3. In the top panel, the red curve shows the best fit using a modified FRED curve to accommodate a plateau at the peak.

At 95 s, the flux increases by a factor of three to four and is then followed by a smooth decay that is not well fit by an exponential curve. Figure 3 shows that, instead, it is better described by a power law, as expected in burst tails when

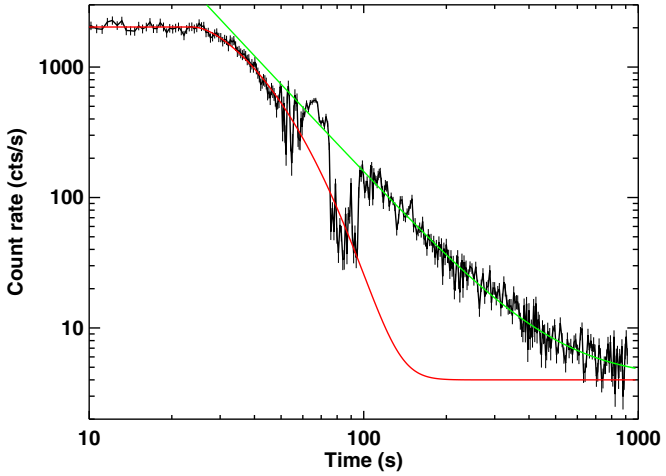

Figure 3. Burst decay light curve in the 3–30 keV band, with 0.5 s, 1 s, 2 s, 4 s, and 8 s bins, in the 0–60 s, 60–120 s, 120–240 s, 240–480 s, and 480–1000 s ranges, respectively. The red curve shows the modified FRED curve fit to the 0–50 s interval of the light curve (identical to the model presented in Figure 2), and the green curve shows a power-law fit to the 110–900 s interval. Both models include a constant equal to 4 counts s^{-1} to account for the persistent emission.

nuclear reactions no longer take place (in't Zand et al. 2014 and references therein). Fitting to the burst tail (110–900 s) a function defined as

$$f(t) = C_0 \left(\frac{t - t_s}{t_0 - t_s} \right)^{-\alpha} \quad (2)$$

and setting the time of the first point in the fit $t_0 = 110$ s (C_0 is the count rate at t_0, and t_s is the time of the burst onset), we find a decay index $\alpha = 2.25 \pm 0.03$. As noticed by in't Zand et al. (2014), α is strongly correlated with t_s; however, we estimate that the error on t_s cannot exceed ± 0.2 s, which leads to a systematic error on α lower than ± 0.002. Despite some variability, the interval from 75 s to 95 s seems to match with the extrapolation of the exponential decay. Another noticeable fact is that the two cooling curves do not intersect. These results are discussed in Section 6.

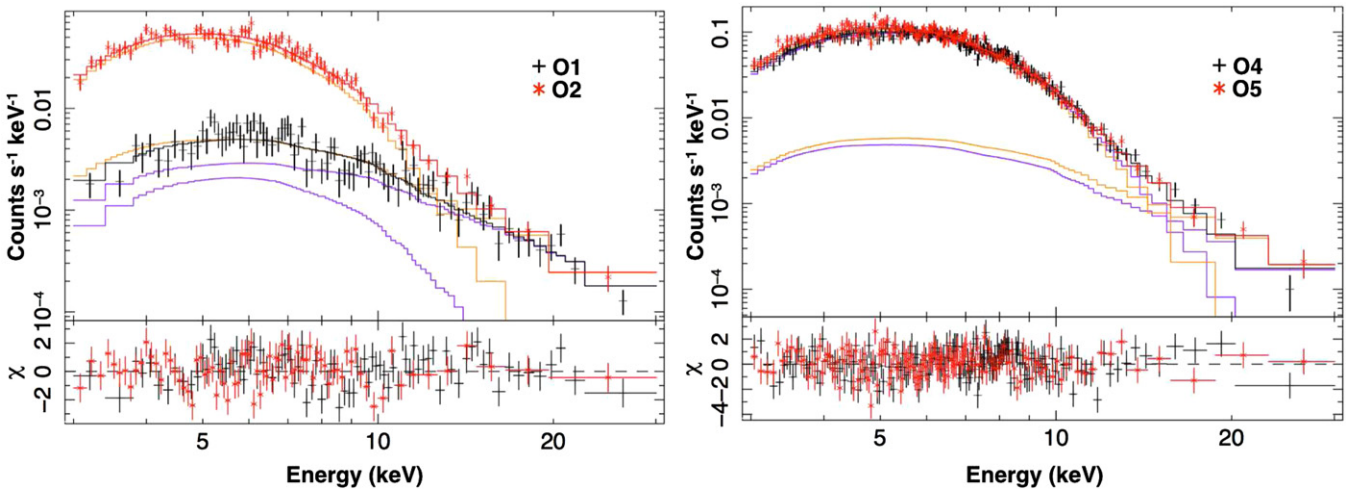

Figure 4. Spectra of the outburst phases with their best-fit model and the decomposition of the model into the blackbody component and the power-law component (high-energy tails). The left panel shows the spectrum of phases O1 (black plus signs, and model breakdown in purple), and O2 (red crosses, and model breakdown in orange). The right panel shows phases O4 (black plus signs, and model breakdown in purple) and O5 (red crosses, and model breakdown in orange). Each spectrum is the combination of data from modules A and B. The data points are shown with 1σ error bars, and the solid lines show the best-fit model. The lower panels show the deviation from the model in units of standard deviation.

Table 1
Outburst Fit Parameters, Flux, Luminosity (assuming $d = 7.0$ kpc), and Derived Accretion Rate per Unit Area at the NS Surface for the Different Phases Identified in Section 3

Outburst Phase	$k_B T$ (keV)	Γ	F_{2-10}[a]	F_b[b]	L_b[c]	$\dot{m}$[d]	$\dot{m}_{\rm Edd}$[e]	$\dot{M}$[f]
O1	$1.74^{+0.66}_{-0.30}$	$1.27^{+0.31}_{-0.40}$	$0.184^{+0.015}_{-0.014}$	$0.987^{+0.144}_{-0.145}$	$0.579^{+0.084}_{-0.085}$	32.4	3.6×10^{-4}	0.64
O2	1.35 ± 0.05	$1.50^{+0.73}_{-0.97}$	$3.01^{+0.13}_{-0.12}$	$5.21^{+0.42}_{-0.40}$	$3.06^{+0.25}_{-0.23}$	171	1.9×10^{-3}	3.4
O4	1.46 ± 0.03	$1.69^{+0.72}_{-0.97}$	5.58 ± 0.18	$8.04^{+0.38}_{-0.35}$	$4.71^{+0.22}_{-0.21}$	264	3.0×10^{-3}	5.3
O5	1.39 ± 0.04	$1.57^{+0.98}_{-1.49}$	$6.16^{+0.22}_{-0.21}$	$9.14^{+0.52}_{-0.48}$	$5.36^{+0.30}_{-0.28}$	300	3.4×10^{-3}	6.0

Notes.
[a] Unabsorbed 2–10 keV flux in units of 10^{-11} erg cm^{-2} s^{-1}.
[b] Unabsorbed bolometric flux (evaluated over the 0.1–100 keV energy range) in units of 10^{-11} erg cm^{-2} s^{-1}.
[c] Unabsorbed bolometric luminosity assuming a distance of 7 kpc in units of 10^{35} erg s^{-1}.
[d] Accretion rate per unit area in g cm^{-2} s^{-1} determined with Equation (3).
[e] Accretion rate per unit area normalized by the Eddington accretion rate $\dot{m}_{\rm Edd} = 8.8 \times 10^4$ g cm^{-2} s^{-1} (assuming $M = 1.4\,M_\odot$ and $R = 10$ km).
[f] Global accretion rate in units of $10^{-11}\,M_\odot$ yr^{-1}, assuming an NS radius of 10 km.

4. OUTBURST

We fit the four different phases of outburst identified in Section 3 (first observation, and low level, pre-burst and post-burst in the second observation: O1, O2, O4, O5, respectively) with an absorbed blackbody + power-law model (`TBabs` × (`bbody` + `powerlaw`)) with tied column density. This model is physically interpreted as the thermal emission of the disk and the NS surface (in the present case, these two components are indistinguishable and are thus modeled with a single blackbody) in addition to the non-thermal emission from a corona (Compton scattering of thermal photons by hot electrons). We obtain good agreement between the model and the data with a $\chi^2_\nu = 1.15$ (461 dof), yielding a column density $N_{\rm H} = 8.3^{+1.9}_{-1.3} \times 10^{22}$ cm^{-2} (Figure 4). The blackbody temperatures and power-law photon indices are presented in Table 1, along with the corresponding bolometric fluxes, luminosities, and derived accretion rates.

The column density that we find is low compared to previous studies. For instance, Muno et al. (2003) found $N_{\rm H} = (9.7 \pm 0.2) \times 10^{22}$ cm^{-2} using 2–7 keV data from *Chandra*, Trap et al. (2009) found $N_{\rm H} = (11.9 \pm 0.2) \times 10^{22}$ cm^{-2} using 2–8 keV data from *XMM-Newton*, and Degenaar & Wijnands (2010) found $N_{\rm H} = (14.0 \pm 0.7) \times 10^{22}$ cm^{-2} using 2–10 keV data from *Swift*/XRT. In these works, the results were obtained using the default XSPEC cross-sections and abundances, which leads to $N_{\rm H}$ values ≈33% lower than those obtained with `TBabs` using Wilms et al. (2000) abundances and Verner et al. (1996) cross-sections (Nowak et al. 2012). However, we note that these past studies were done over smaller energy ranges and used a simple absorbed power-law model, which requires a higher column density than a blackbody to get a curved spectrum at low energies.

The strong gravitational field of the NS decreases the luminosity observed by a distant observer (noted with the subscript ∞) with respect to the one emitted in the local frame (subscript $\star$) by a factor $(1+z)^2$, where $1 + z = (1\text{–}2GM/(R_\star c^2))^{-1/2}$. In this equation, c is the speed of light, M and R are the mass and radius of the NS, and G is the gravitational constant. It also affects the emitted spectrum by changing the temperature observed by a distant observer $T_\infty = T_\star(1+z)^{-1}$ (Lewin et al. 1993).

Assuming the canonical values $M = 1.4\,M_\odot$ and $R_\star = 10$ km, one finds $1+z \approx 1.31$. Unless specifically noted with the subscript $\star$, all physical quantities will hereafter be expressed as seen by a distant observer.

The unabsorbed bolometric luminosity can be converted into an accretion rate per unit area $\dot{m}$ using the formula[11] $L_b = 4\pi R_\star^2 \dot{m}\,(GM/R_\star)(1+z)^{-1}$ (Galloway et al. 2008), which can be inverted to show

$$\dot{m} = 32.8 \times \left(\frac{F_b}{10^{-11}\mathrm{erg\,cm^{-2}\,s^{-1}}}\right)\left(\frac{M}{1.4\,M_\odot}\right)^{-1}\left(\frac{1+z}{1.31}\right) \times \left(\frac{R_\star}{10\,\mathrm{km}}\right)^{-1}\left(\frac{d}{7\,\mathrm{kpc}}\right)^{2}\ \mathrm{g\,cm^{-2}\,s^{-1}}, \quad (3)$$

where d is the distance to the observer and F_b the bolometric flux seen by a distant observer.

5. TYPE I BURST

We first look at the burst spectrum divided into three phases, corresponding to the PRE (0–22.5 s, B1), the high-temperature (after the photosphere falls back onto the NS surface, commonly referred to as *touch-down*, 22.5–41.0 s, B2), and the beginning of the decay (41.0–72.0 s, B3), as defined in the next paragraph. We use the O3 outburst phase (14.6 ks right before the burst) as background. The cross calibration between FPMA and FPMB is excellent, we found agreement to better than 0.2%, so we removed the normalization constant from the model. The three spectra are well fit with an absorbed blackbody (we use `TBabs × bbody`) with tied column density ($\chi^2_\nu = 1.06$, 255 dof, Figure 5). We find $N_\mathrm{H} = (11.3 \pm 1.5) \times 10^{22}$ cm^{-2}, consistent within errors with the value found for the outburst, and blackbody temperatures of 2.11 ± 0.04 keV, 2.65 ± 0.06 keV, and 1.97 ± 0.05 keV for spectra B1, B2, and B3, respectively.

Next we look at the time-resolved spectral properties of the burst. The burst is divided to yield 700 net counts (FPMA + FPMB) in each time slice, from t_s to $t_s + 359$ s. The top panel of Figure 6 shows the luminosity derived from the blackbody fit to the time-resolved spectra, assuming a distance to the source of 7 kpc. The middle panel of Figure 6 shows the blackbody temperature and the bottom panel shows the NS photospheric radius R inferred from the blackbody luminosity L and temperature T:

$$R = \sqrt{\frac{L}{4\pi\,\sigma\,T^4}}, \quad (4)$$

with σ being the Stephan–Boltzmann constant.

Integrating the luminosity over these 32 slices, we find that the total energy radiated is 9.5×10^{39} erg (at 7 kpc). Following Galloway et al. (2008), we calculate the burst characteristic time $\tau = E_b/F_\mathrm{pk}$, where E_b is the fluence of the burst (i.e., the integrated bolometric burst flux) and F_pk is the peak bolometric flux. With $E_b = 1.61 \times 10^{-6}$ erg cm^{-2} and $F_\mathrm{pk} = 3.58 \times 10^{-8}$ erg cm^{-2} s^{-1}, we find $\tau = 45.0$ s. We also note the very large dynamic range of this burst, which appeared on top of weak persistent emission; the ratio of the burst peak bolometric flux to the persistent bolometric flux preceding the burst is 445, amongst the highest ever observed (in't Zand et al. 2014).

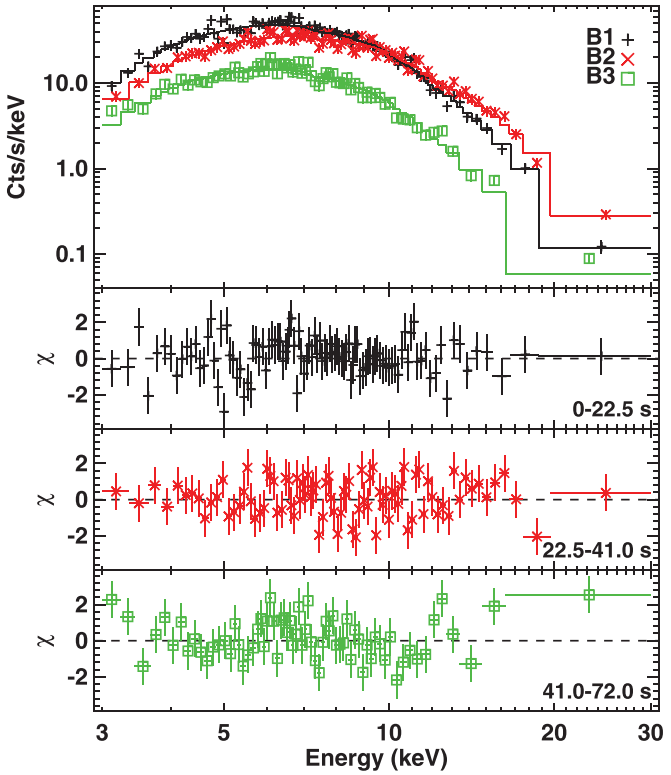

Figure 5. Spectrum of the burst recorded during three time intervals B1 (0–22.5 s, black plus signs), B2 (22.5–41.0 s, red crosses), and B3 (41.0–72.0 s, green squares). Each point is the combination of FPMA and FPMB, and the errors are 1σ. The lower panels show the residuals between the best-fit models (absorbed blackbody) and the data in units of standard deviation.

As pointed out by Worpel et al. (2013), the persistent flux can vary during bursts, which limits the accuracy of our method. We thus tried to apply their analysis to this data set. We subtracted the instrumental background from the burst time-resolved spectra, and fitted them with the model `TBabs ×` (`blackbody` $+ f_a \times$ PE), PE being the best fit model to the persistent emission preceding the burst with all parameters fixed, and f_a being a constant to account for possible variability of the PE. The maximum value of f_a is found during the PRE phase of the burst, however it is very poorly constrained: $f_a = 122^{+154}_{-122}$. This is explained by the fact that the ratio between the PRE emission ($\approx L_\mathrm{Edd}$) and the persistent emission ($3 \times 10^{-3} L_\mathrm{Edd}$) is about 333, while the two spectra have fairly similar shapes allowing the persistent spectrum to "nest" into the burst spectrum without any constraint on f_a. We thus are not able to constrain the PE variability during the burst.

5.1. Presence of an Absorption Line

We observe the presence of a weak transient spectral feature during the PRE, shown in Figure 7. We tested an absorption edge to model the feature but it did not fit, returning a null depth. The best fit is obtained using a narrow (poorly constrained width) Gaussian absorption line centered at 5.46 ± 0.10 keV, which only marginally improves the χ^2_ν from 1.02 (216 dof) to 0.99 (213 dof), keeping N_H fixed to 1.13×10^{23} cm^{-2} in both cases. The Gaussian normalization parameter is -0.029 ± 0.016 photon cm^{-2} s^{-1}, yielding an equivalent width of 0.08 ± 0.06 keV.

[11] This equation assumes that the total luminosity of the system is powered by accretion (i.e., emission from the accretion disk, the corona and the NS surface), and that obscuration is negligible. This is equivalent to saying that the radiation efficiency is equal to 1.

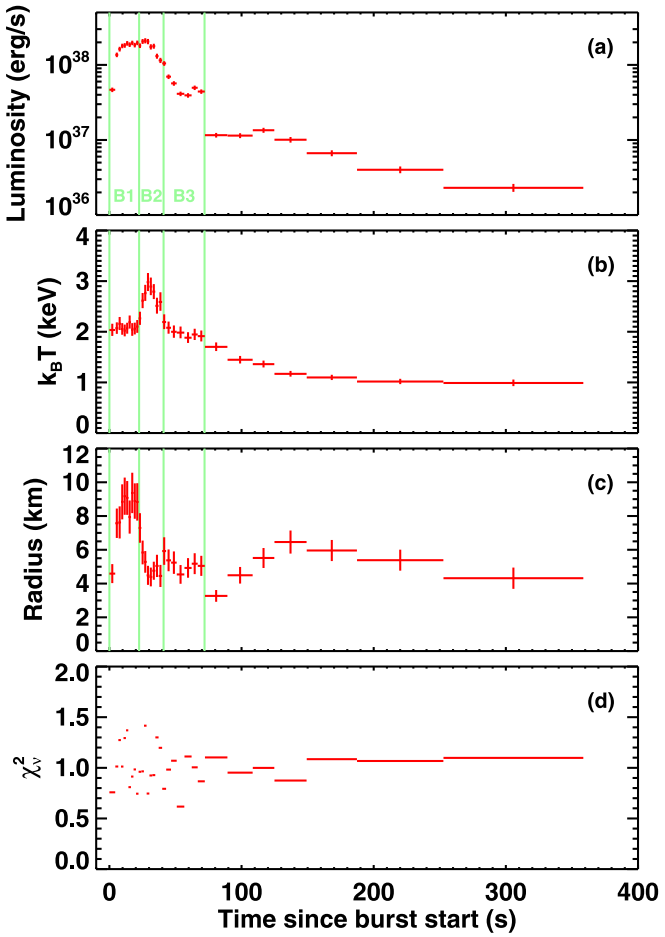

Figure 6. Time-resolved blackbody spectral fit of the burst, assuming a distance of 7 kpc to the source, and keeping the column density fixed to 1.13×10^{23} cm^{-2}. Panel (a) shows the bolometric blackbody luminosity. Panel (b) shows the blackbody temperature, and panel (c) shows the neutron star photospheric radius inferred from the blackbody flux and temperature. Panel (d) shows the reduced χ^2 of each fit. All quantities are as seen by a distant observer. The green vertical lines define the three time intervals B1, B2, and B3 used in Figure 5.

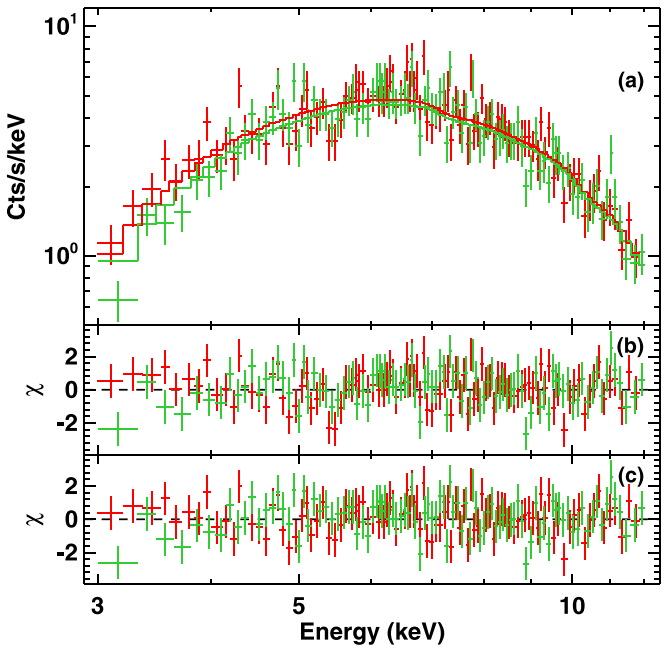

Figure 7. FPMA (red) and FPMB (green) spectra of the burst during time interval B1 (the PRE phase), with 1σ error bars. Panel (a) shows the data with the absorbed blackbody best-fit model, and panel (b) shows the residuals for this model in units of standard deviation. Panel (c) shows the residuals when a Gaussian absorption line at 5.46 keV is added to the model.

We first performed a sanity check using a much smaller region of 60″ radius, which makes it less sensitive to background variations. The line was still visible with this reduced extraction region. Next, we determine the significance using the XSPEC (Arnaud 1996) script `simftest`[12] with 5000 trials (constraining the line centroid in the 5.26–5.66 keV range, and the line width to be <0.05 keV), we found that the probability for the absorption line to be required by the data is 98.5% (equivalent to 2.4σ, as it is a one-sided distribution). This test was performed with the model `constant` × `TBabs` × (`BBody` + `Gauss`) jointly fit to FPMA and FPMB spectra over the 3–15 keV range, with $N_{\rm H}$ fixed to 1.13×10^{23} cm^{-2}. The spectra are rebinned to at least 25 counts and 3σ per bin (the former condition insures a bin significance higher than 5σ in the 5–6 keV range), as shown in Figure 7. Accounting for the fact that we found the line in one of three sub-spectra (spectra B1, B2, B3), the significance of the line drops to 95.6% (1.7σ).

5.2. Search for Oscillations

In 1996 April and July, Strohmayer et al. (1997) reported strong detection of oscillations at a frequency of 589 Hz during three bursts observed with *RXTE* coming from a direction close to GRS 1741.9-2853. The strongest oscillations were detected during the brightest of the three bursts with a fraction[13] of (8.4 ± 1.4)% during the peak and (18.4 ± 2.8)% during the decay, and were seen only above 8 keV. These bursts were tentatively attributed to MXB 1743–29 (an LMXB 24′ away from GRS 1741.9-2853), with the 99% confidence region excluding the position of GRS 1741.9-2853. In 1996 August–September, Cocchi et al. (1999) observed the Galactic center with *BeppoSAX* and detected three bursts from GRS 1741.9-2853, determining that it is a transient LMXB. Galloway et al. (2008) made the association between GRS 1741.9-2853 and the oscillations detected by Strohmayer et al. (1997) because these bursting episodes happened only a few months apart, and had similar characteristics.

We ran a combination of timing analysis procedures in order to look for coherent pulsations in the *NuSTAR* data set. One difficulty with *NuSTAR* timing is dead time: each event is followed by a dead time of ≈2.5 ms (Harrison et al. 2013). At high count rates, such as those reached during the burst in our observation, dead time affects the frequency response of the FPMs, producing a "wavy" pattern in the power density spectrum (PDS; van der Klis 1989; Zhang et al. 1995), which affects heavily our detection limits for pulsations.

We first analyzed the burst light curve with a running-window epoch folding (Leahy et al. 1983) around 589 Hz. We used

[12] simftest is a script that generates fake spectra based on the model *without* the component under investigation, and then fit to them the model with and without the component. The difference in fit statistics is recorded for each trial and is then compared to the difference obtained with the actual data set. If a significant number of trials return a difference in fit statistics larger than that obtained with the real data set, we conclude that the component under investigation is not required by the data, as the spectral feature likely results from a statistical fluctuation.

[13] Defined as the amplitude of the sinusoid divided by the constant count rate below the oscillations.

a number of different windows (over the range 2–400 s) and calculated the χ^2 of the putative pulse profiles. We found no signals exceeding the 90% detection level, taking into account the number of trial periods per interval and the number of time intervals that the burst was divided into (Leahy et al. 1983). We then searched for pulsations at any frequency during the burst. To work around the distortions of the white noise level of the PDS due to dead time, we followed Bachetti et al. (2014) and used the co-spectrum as a proxy for the PDS: the Fourier transform of the signal from FPMA is multiplied by the conjugate of the signal from FPMB, producing the cross PDS, which contains in its real part (or co-spectrum) the signal that is correlated between the two FPMs. Since the per-event dead time is uncorrelated between the two detectors, the co-spectrum does not show the deformations of the white noise level that affect the PDS.

We analyzed the *dynamical* co-spectrum during the burst, looking for transient peaks that might indicate a pulsation over intervals of 2–100 s in a sliding window. The burst, and in particular its rising and decay phases, were scrutinized, as well as the entire observation covering the different outburst phases. We searched for pulsations in the 3–30 keV and 8–30 keV bands. We did not find any significant power at any frequency (following the method of van der Klis 1989, and taking into account the prescription in Bachetti et al. 2014), which means that we did not detect any pulsation in the burst nor in the outburst phases. The only variability found during the burst was a strong increase of the red noise level, as it is expected from burst light curves (e.g., Terrell & Olsen 1970).

To estimate upper limits, we simulated a large number of event lists containing a sinusoidal pulsation, with the observed count rates and durations for each interval (B1, B2, B3, burst tail), and estimated the pulsed fraction for which the signal was detected 90% of the time above the Leahy et al. (1983) detection level for the relevant technique (epoch folding, assuming $n_{\rm trials} = 1000$ or PDS/cospectrum). We find that our upper limits at 589 Hz, calculated with epoch folding are always comparable or above the pulsed fraction measured by Strohmayer et al. (1997; ∼20% in B1 and B2, going to 25% in B3 and in the burst tail), and therefore we cannot rule out the presence of these oscillations in our data set. Regarding the search at all frequencies, the upper limit depends on the frequency, particularly because of the suppression of low frequency modulation in dead time affected data sets (see Bachetti et al. 2014). At high frequencies (∼600 Hz), the upper limits are similar to those determined with epoch folding, at low frequencies (∼50 Hz), the upper limit is higher in the high-count rate intervals, 30%–40% for B1 and B2.

6. DISCUSSION

Figure 6 shows indications of PRE during the first 20 s of the burst, where the temperature is constant at ≈2.1 keV. The sudden increase in temperature that follows is interpreted as the "touch down," when the photosphere falls back onto the NS. This is far from being an extreme PRE event, as the X-ray flux remains measurable during the expansion phase (the adiabatic cooling can be so extreme in the case of super-expansion bursts that the bulk of the flux moves into the UV band), and the apparent blackbody radius[14] does not exceed 10 km (Figure 6), but the constant bolometric flux and the blackbody temperature evolution (which determine the apparent blackbody radius; see Equation (4)) are clearly suggestive of a PRE.

[14] Not corrected for the relativistic effects.

The value of $\tau = 45.0$ s that we determined in Section 5 puts this burst in the category of the long and unusual ones for this source, most of its "regular" bursts having $\tau \sim 10$ s (Galloway et al. 2008). This is not to be confused with super-bursts lasting longer than 1 hr, which results from the slow burning of C (e.g., Strohmayer & Brown 2002), nor with intermediate bursts lasting ∼30 minutes, thought to arise from the burning of a thick layer of pure He (e.g., in't Zand et al. 2005).

GRS 1741.9-2853 is known to produce both pure He and mixed H/He bursts (Trap et al. 2009). The accretion rate increased during our two observations to reach 0.003 $\dot{m}_{\rm Edd}$ before the burst, well below the critical value $\dot{m}_C = 0.01\,\dot{m}_{\rm Edd}$ for which there is no stable burning of the freshly accreted H, nor of the He, assuming solar CNO abundance ($Z_{\rm CNO}$; Fujimoto et al. 1981; Bildsten 1998; Narayan & Heyl 2003). We note that $\dot{m}_C$ is proportional to ${Z_{\rm CNO}}^{1/2}$, i.e., only weakly dependent on our assumption of solar abundance (see Equation (36) in Bildsten 1998). Peng et al. (2007) show that once a sufficient column density is reached, unstable H burning can trigger the burning of a thick He layer that formed by sedimentation for $\dot{m} \lesssim 0.003\,\dot{m}_{\rm Edd}$, resulting in a powerful long burst. This matches well with what we observed; Hydrogen burning is β-limited, which slows down the reaction compared to helium burning, hence creating a longer burst. However, the burst would have been much weaker if only H had burned. Thus, based on the relatively long duration of the burst and on the low accretion rate preceding the burst, we conclude that we observed an H-triggered, mixed H/He burst.

The conclusion that this burst was H-rich is now used to calculate the corresponding Eddington luminosity, allowing us to determine a distance for GRS 1741.9-2853. In the case of a PRE burst, the peak flux $F_{\rm pk}$ corresponds to the Eddington luminosity $L_{\rm Edd}$, and the distance d of the object is simply given by

$$d = \left(\frac{L_{\rm Edd}}{4\pi\ F_{\rm pk}}\right)^{1/2}.$$

The Eddington luminosity, as seen by a distant observer, is given by (Lewin et al. 1993)

$$L_{\rm Edd} = \left(\frac{4\pi c G M_{\rm NS}}{\kappa}\right)(1+z)^{-1},$$

where κ is the electron scattering opacity during the expansion phase. In the case where the scattering electrons become relativistic, the opacity can be approximated by $\kappa = 0.2 \times (1+X)[1+(kT/39.2\,{\rm keV})^{0.86}]^{-1}$ cm^2 g^{-1}, where X is the hydrogen mass fraction in the photosphere (Lewin et al. 1993). Following the assumption that we observed a H-rich burst, we use $X = 0.7$ (corresponding to solar composition) and find $L_{\rm Edd} = 1.7 \times 10^{38}$ erg s^{-1}. In the time-resolved spectral analysis of the burst, we found that the brightest slice has a bolometric flux $F_{\rm pk} = 3.58^{+0.29}_{-0.28} \times 10^{-8}$ erg cm^{-2} s^{-1}, which leads to a distance of 6.3 ± 0.5 kpc. Table 2 summarizes the distances that have been found in past studies for this source, and shows the dependency of the distance on the Eddington luminosity. The present peak flux is consistent with the brightest bursts that have been observed for this source in the past. Our distance measurement is consistent with the lower range that had been established by Cocchi et al. (1999), Galloway et al. (2008), and Trap et al. (2009).

The largest source of uncertainty in this calculation is the hydrogen mass fraction X chosen for the NS atmosphere in the Eddington luminosity calculation, where any X value lower

Table 2
Distance for GRS 1741.9-2853 from This Study Compared to Past Work

Reference	$F_{\rm pk}$ (10^{-8} erg cm^{-2} s^{-1})	d (kpc) $L_{\rm Edd}$ ($X = 0.7$)	d (kpc) $L_{\rm Edd}$ ($X = 0$)	d (kpc) $L_{\rm Edd}$ (Kuulkers)
Cocchi et al. (1999)	3.26 ± 0.26	$^{*}6.65 \pm 0.53$	$^{*}8.67 \pm 0.69$	9.87 ± 0.79
Galloway et al. (2008)	3.80 ± 1.0	$^{*}6.16 \pm 1.6$	$^{*}8.03 \pm 2.1$	9.14 ± 2.4
Trap et al. (2009)	$5.5^{+0.7}_{-2.1}$	$<5.12^{+2.0}_{-0.65}$	$<6.68^{+2.5}_{-0.85}$	$^{*}<7.60^{+2.9}_{-0.97}$
This work	$3.58^{+0.29}_{-0.28}$	$^{*}6.35^{+0.50}_{-0.51}$	$8.27^{+0.65}_{-0.66}$	$9.42^{+0.74}_{-0.75}$

Notes. The second column shows the burst peak bolometric flux that the different studies used for their distance measurement. The three rightmost columns show the distance they obtained for different values of the Eddington luminosity: 1.7×10^{38} erg s^{-1} for $X = 0.7$, 2.9×10^{38} erg s^{-1} for $X = 0$, and $(3.79 \pm 0.15) \times 10^{38}$ erg s^{-1} as determined empirically by Kuulkers et al. (2003). The stars indicate which value of the Eddington luminosity was favored in each study.

than 0.7 would place the source further (Table 2). Uncertainty on the distance also comes from the NS mass; for instance, considering $M = 2\,M_{\odot}$ leads to a distance 9.2% larger. Given these uncertainties, our distance of 6.3 ± 0.5 kpc should be regarded as a lower limit, consistent with the value of $d = 7$ kpc that we have been using throughout this paper. Our measurement of the column density toward GRS 1741.9-2853 ($\sim 10^{23}$ cm^{-2}) is consistent with the source being closer than the Galactic center (*NuSTAR* measured $N_{\rm H} = 1.66^{+0.70}_{-0.61} \times 10^{23}$ cm^{-2} to the Galactic center during flares from Sagittarius A*; Barrière et al. 2014).

Transient achromatic variability is observed between 48 s and 75 s into the burst. The variability is mostly on top of the exponential decay trend, but we can see at 52 s and 54.5 s that the flux goes below the decaying trend, suggesting that transient obscuration is taking place. It is hard to determine if the interval between 75 s and 95 s belongs to the exponential decay trend, or if it is part of the power-law decay with obscuration (Figure 3). The latter option might be more physical, as it is hard to explain why the flux would have suddenly risen by a factor three to four while transitioning from exponential to power-law cooling. However, the fact that the two curves do not intersect could be an indication that re-heating of the NS took place during the episode of variability.

GRS 1741.9-2853 already displayed such late-time variability, as visible in bursts No. 3 and possibly 4 observed by *INTEGRAL* JEM-X (although the features were not discussed; Trap et al. 2009). in't Zand et al. (2011) suggest that this variability is caused by clouds of electrons in thermal balance with the radiation field scattering the NS thermal emission (Thomson scattering). The clouds are orbiting the NS and alternatively obscure our line of sight and reflect the NS radiation toward us. The presence of these clouds could be explained by the reorganization of the accretion disk that had been disrupted by the burst. To our knowledge, this phenomenon has been reported in only six bursts from other systems, all showing super-expansion, where the photosphere is lifted up to thousands of km off the NS surface (van Paradijs et al. 1990; Strohmayer & Brown 2002; Molkov et al. 2005; in't Zand et al. 2005, 2011; Degenaar et al. 2013a). It is interesting that the present burst shows similar behavior, although the photosphere has been merely lifted to a few tens of kilometers. Assuming that the two troughs at 52 s and 54.5 s are the signature of a cloud in a Keplerian orbit of period $P = 2.5$ s, their elevation above the NS surface would be $(P^2GM/4\pi^2)^{1/3} \approx 3 \times 10^3$ km (for $M = 1.4\,M_{\odot}$), well beyond the photosphere. Thus, if this variability was indeed the sign of a disturbed inner accretion disk, it would have been caused only by the action of the Eddington flux and the resulting X-ray heating (e.g., Ballantyne & Everett 2005). The fact that late time variability is rare could then be explained by the viewing angle, where only high inclination systems would show this phenomenon. We note however, that GRS 1741.9-2853 is not an eclipsing or dipping system, which limits the validity of this explanation.

The high dynamic range of this burst allows the observation of a long power-law decay tail, starting around $t = 110$ s after the variability ceased. This is consistent with a pure radiative cooling without any additional production of heat. We find a power-law index of 2.25, which indicates that photons contributed significantly to the heat capacity (in't Zand et al. 2014).

Oscillations at 589 Hz had been tentatively associated to GRS 1741.9-2853 (Section 5.2). Despite *NuSTAR*'s ability to measure oscillation frequency up to $\approx$1 kHz (over short periods of time; Bachetti et al. 2014), we did not detect oscillations in the burst nor in the outburst. However, our upper limits are not constraining, being always above the pulsed fraction measured by Strohmayer et al. (1997). In addition, it has been proposed that oscillations appear mostly in He burning runaways (Cumming & Bildsten 2000; Narayan & Cooper 2007), which was not the case here, and it is known that they are not detected consistently even in He bursts from sources known to produce pulsed emission. So we cannot confirm nor repudiate the association of the 589 Hz pulsation with GRS 1741.9-2853.

The spectrum of the PRE phase shows weak evidence of an absorption line at 5.46 ± 0.10 keV (95.6% confidence level). Although this is only marginal detection, the importance of these features makes it worthwhile to consider its interpretation. One additional motivation for this is that there is a precedent: a line at 5.7 ± 0.25 keV was detected in the rise and PRE phase of a bright burst from 4U 1636-536 observed with *Tenma* a.k.a. *Astro-B* (Waki et al. 1984). Although this detection was clear (>99.5% confidence level), no similar line was ever observed subsequently in any source.

Detection of absorption lines in burst spectra are rare and have been controversial due to their lack of consistency, even within seemingly identical bursts from given sources. Here is a brief summary of the main cases. A line at 4.1 keV was detected in the *Tenma* spectra of non-PRE bursts from 4U 1636-536 (in 4 out of 12 bursts; Waki et al. 1984) and from 4U 1608-52 (in 3 out of 17 bursts; Nakamura et al. 1988). Another line at 4.1 keV was found by Magnier et al. (1989) with *EXOSAT* in a 0.5 s slice of the rise of a non-PRE burst from EXO 1747-214, although this detection is more controversial due to its short duration and large equivalent width. More recently, Cottam et al. (2002) found a set of absorption lines in the stacked spectra of 28 bursts from EXO 0748–676 observed with the Reflection Grating Spectrometer

Table 3
Kα$_1$ Transition Energy of H-like Ions *Possibly* Present in the Atmosphere of the NS, and Corresponding Division Factor to Shift the Line to 5.46 keV

Ion	$E_{K\alpha}$ (keV)	$(1+z)$
Zn	9.31	1.71
Ni	8.10	1.48
Fe	6.97	1.28
Mn	6.44	1.18
Cr	5.93	1.09
V	5.44	1.00

onboard *XMM-Newton*, which they interpreted as being due to transitions from Fe XXV, Fe XXVI, and O VIII, all gravitationally redshifted by a factor $1+z=1.35$. This detection was not confirmed in subsequent observations (Cottam et al. 2008), and a 552 Hz spin was found for the NS (Galloway et al. 2010), which is incompatible with the production of narrow absorption lines at the surface of an NS (Lin et al. 2010). in't Zand & Weinberg (2010) analyzed 32 super-expansion bursts and detected absorption edges in three cases. They interpreted them as signatures of heavy elements (synthesized during the burst) present in the atmosphere of the NS and the wind created by the burst.

If the GRS 1741.9-2853 line is real, what could its origin be? The two mechanisms that can produce absorption lines are resonant cyclotron scattering and resonant atomic level transitions. An electron cyclotron line at 5.5 keV would require a magnetic field of the order of 10^{12} G, which is three to four orders of magnitude higher than what is expected for Type I bursters (e.g., Bildsten 1998). Thus, we favor the resonant atomic transition interpretation.

During the PRE phase of the present burst, we observe a roughly constant color temperature of $T=2.44\times10^7$ K ($k_BT=2.1$ keV), which corresponds to a local effective temperature of $T_{e\star}\approx23$ MK, using a correction factor of 1.4 to account for the spectral hardening from Comptonization (Madej et al. 2004), and correcting for the redshift with $1+z=1.31$. We assume that accretion is quenched during the PRE phase of the burst due to the radiation pressure at the Eddington level. Weinberg et al. (2006) showed that the products of nuclear burning can come to sufficiently shallow depth to be blown away by the wind and therefore be exposed to the photosphere. According to the same authors, the most likely heavy elements to be present in the photosphere and above it in the wind are Zn and Cr for a mixed H/He burst. At a temperature of $T_{e\star}\approx23$ MK, Saha equilibrium indicates that these elements will be either fully ionized or in the H-like ionization state. The most intense transition for H-like ions is Kα.[15] We see in Table 3 that if Zn was causing this absorption line, the gravitational redshift factor would be $1+z=1.70$, which is not reasonable during a PRE phase. However, Cr yields a factor $1+z=1.09$, resulting in a plausible radius range of 29.0–41.4 km for a mass range of 1.4–2.0 $M_\odot$.

Besides the obvious limitation that the line is only weakly detected, one caveat of this interpretation is that the accretion rate preceding this burst was lower than $0.01\,\dot{m}_{\rm Edd}$. This goes beyond the case studied by Weinberg et al. (2006; accretion rate of $\approx0.01\,\dot{m}_{\rm Edd}$ resulting in a mixed H/He burst triggered by triple-α He reactions), which could result in very different nucleosynthesis products being sent in the NS atmosphere.

[15] The Kα transition is actually double, Kα$_1$ referring to $1s\rightarrow2p_{3/2}$ and Kα$_2$ referring to $1s\rightarrow2p_{1/2}$, with Kα$_1$ twice as strong as Kα$_2$. However, the energy difference is too small to differentiate with *NuSTAR*.

7. SUMMARY

NuSTAR observed GRS 1741.9-2853 twice in summer 2013 as it was entering in outburst for the first time since 2010 July. We detected a Type I burst with the second highest fluence reported for this source (burst No. 8 in Galloway et al. (2008) has 50% higher fluence). Based on the low accretion rate before the burst ($3.0\times10^{-3}\,\dot{m}_{\rm Edd}$) and the long duration of the burst, which includes a 18 s plateau, we interpret it as an H-triggered mixed H/He thermonuclear explosion. The burst underwent a moderate phase of PRE, thus reaching the Eddington luminosity.

Assuming an H-rich atmosphere, we derive a new constraint on the source distance, 6.3 ± 0.5 kpc. However, given the fact that this value relies on highly uncertain parameters, such as the hydrogen mass fraction in the atmosphere, and the NS mass, we consider it more conservative to use the distance of 7 kpc, in agreement with past works.

The low persistent emission allows a power-law decay to be revealed in the burst tail. The transition from the exponential to the power-law decay is affected by strong variability above and below the decay trend. To our knowledge, it is the first time that this phenomenon is reported in a moderate PRE burst. The current model involving clouds of electrons created as the inner accretion disk reorganizes itself after having been disturbed by the burst is hard to reconcile with the fact that this late time variability is rare.

We searched for pulsations during the burst and the outburst, but found none. However our upper limits on the pulsed fraction around 589 Hz (between 17% and 25%) during the peak and the decay of the burst are not constraining as they are above the strongest pulsed fraction reported by Strohmayer et al. (1997).

A line at 5.46 ± 0.10 keV is weakly detected during the PRE phase of the burst. Assuming that the line is real, we speculate that it is due to the Kα resonance absorption line of H-like Cr ions, which is a product of the nuclear reactions, based on the work of Weinberg et al. (2006). Unfortunately, given that the line is observed while the atmosphere is lifted off the surface by radiation pressure, its gravitational redshift carries no information about the NS mass and radius.

This work was supported under NASA contract No. NNG08FD60C, and made use of data from the *NuSTAR* mission, a project led by the California Institute of Technology, managed by the Jet Propulsion Laboratory, and funded by the National Aeronautics and Space Administration. We thank the *NuSTAR* Operations, Software and Calibration teams for support with the execution and analysis of these observations. This research has made use of the *NuSTAR* Data Analysis Software (NuSTARDAS) jointly developed by the ASI Science Data Center (ASDC, Italy) and the California Institute of Technology (USA). The authors thank Nevin Weinberg for useful discussions, and the anonymous referee for constructive comments.

Facility: NuSTAR

REFERENCES

Arnaud, K. A. 1996, in ASP Conf. Ser. 101, Astronomical Data Analysis Software and Systems V, ed. G. H. Jacoby & J. Barnes (San Francisco, CA: ASP), 17

Bachetti, M., Harrison, F. A., Cook, R., et al. 2014, ApJ, submitted (arXiv:1409.3248)

Ballantyne, D. R., & Everett, J. E. 2005, ApJ, 626, 364

Barrière, N. M., Tomsick, J. A., Baganoff, F. K., et al. 2014, ApJ, 786, 46
Bildsten, L. 1998, in NATO ASIC Proc. 515: The Many Faces of Neutron Stars, ed. R. Buccheri, J. van Paradijs, & A. Alpar (Dordrecht, Kluwer Academic), 419
Chenevez, J., Kuulkers, E., Beckmann, V., et al. 2009, ATel, 2235
Cocchi, M., Bazzano, A., Natalucci, L., et al. 1999, A&A, 346, L45
Cottam, J., Paerels, F., & Mendez, M. 2002, Natur, 420, 51
Cottam, J., Paerels, F., Méndez, M., et al. 2008, ApJ, 672, 504
Cumming, A., & Bildsten, L. 2000, ApJ, 544, 453
Damen, E., Magnier, E., Lewin, W. H. G., et al. 1990, A&A, 237, 103
Degenaar, N., Miller, J. M., Wijnands, R., Altamirano, D., & Fabian, A. C. 2013a, ApJL, 767, L37
Degenaar, N., Reynolds, M. T., Miller, J. M., et al. 2013b, ATel, 5246
Degenaar, N., & Wijnands, R. 2010, A&A, 524, A69
Degenaar, N., Wijnands, R., Kennea, J. A., & Gehrels, N. 2010, ATel, 2770
Degenaar, N., Wijnands, R., Reynolds, M. T., et al. 2014, in IAU Symp. 303, The Galactic Center: Feeding and Feedback in a Normal Galactic Nucleus, ed. L. O. Sjouwerman, C. C. Lang, & J. Ott (Cambridge: Cambridge Univ. Press), 315
Fujimoto, M. Y., Hanawa, T., & Miyaji, S. 1981, ApJ, 247, 267
Galloway, D. K., Lin, J., Chakrabarty, D., & Hartman, J. M. 2010, ApJL, 711, L148
Galloway, D. K., Muno, M. P., Hartman, J. M., Psaltis, D., & Chakrabarty, D. 2008, ApJS, 179, 360
Grimm, H.-J., Gilfanov, M., & Sunyaev, R. 2002, A&A, 391, 923
Harrison, F. A., Craig, W. W., Christensen, F. E., et al. 2013, ApJ, 770, 103
Houck, J. C., & Denicola, L. A. 2000, in ASP Conf. Ser. 216, Astronomical Data Analysis Software and Systems IX, ed. N. Manset, C. Veillet, & D. Crabtree (San Francisco, CA: ASP), 591
in't Zand, J. J. M., Cumming, A., Triemstra, T. L., Mateijsen, R. A. D. A., & Bagnoli, T. 2014, A&A, 562, A16
in't Zand, J. J. M., Cumming, A., van der Sluys, M. V., Verbunt, F., & Pols, O. R. 2005, A&A, 441, 675
in't Zand, J. J. M., Galloway, D. K., & Ballantyne, D. R. 2011, A&A, 525, A111
in't Zand, J. J. M., & Weinberg, N. N. 2010, A&A, 520, A81
Kennea, J. A. 2009, ATel, 2236
King, A. R., & Wijnands, R. 2006, MNRAS, 366, L31
Kuulkers, E., Chenevez, J., Wijnands, R., et al. 2013, ATel, 5332
Kuulkers, E., den Hartog, P. R., in't Zand, J. J. M., et al. 2003, A&A, 399, 663
Lasota, J.-P. 2001, NewAR, 45, 449
Lattimer, J. M., & Prakash, M. 2001, ApJ, 550, 426
Leahy, D. A., Elsner, R. F., & Weisskopf, M. C. 1983, ApJ, 272, 256
Lewin, W. H. G., van Paradijs, J., & Taam, R. E. 1993, SSRv, 62, 223
Lin, J., Özel, F., Chakrabarty, D., & Psaltis, D. 2010, ApJ, 723, 1053
Liu, Q. Z., van Paradijs, J., & van den Heuvel, E. P. J. 2007, A&A, 469, 807
Madej, J., Joss, P. C., & Różańska, A. 2004, ApJ, 602, 904
Magnier, E., Lewin, W. H. G., van Paradijs, J., et al. 1989, MNRAS, 237, 729
Molkov, S., Revnivtsev, M., Lutovinov, A., & Sunyaev, R. 2005, A&A, 434, 1069
Muno, M. P., Baganoff, F. K., & Arabadjis, J. S. 2003, ApJ, 598, 474
Muno, M. P., Wijnands, R., Wang, Q. D., et al. 2007, ATel, 1013
Nakamura, N., Inoue, H., & Tanaka, Y. 1988, PASJ, 40, 209
Narayan, R., & Cooper, R. L. 2007, ApJ, 665, 628
Narayan, R., & Heyl, J. S. 2003, ApJ, 599, 419
Nowak, M. A., Neilsen, J., Markoff, S. B., et al. 2012, ApJ, 759, 95
Osaki, Y. 1974, PASJ, 26, 429
Özel, F. 2006, Natur, 441, 1115
Peng, F., Brown, E. F., & Truran, J. W. 2007, ApJ, 654, 1022
Porquet, D., Grosso, N., Goldwurm, A., et al. 2007, ATel, 1058
Revnivtsev, M., Lutovinov, A., Churazov, E., et al. 2008, A&A, 491, 209
Sakano, M., Koyama, K., Murakami, H., Maeda, Y., & Yamauchi, S. 2002, ApJS, 138, 19
Strohmayer, T., & Bildsten, L. 2006, New Views of Thermonuclear Bursts (Cambridge: Cambridge Univ. Press), 113
Strohmayer, T. E., & Brown, E. F. 2002, ApJ, 566, 1045
Strohmayer, T. E., Jahoda, K., Giles, A. B., & Lee, U. 1997, ApJ, 486, 355
Sunyaev, R. 1990, IAU Circ., 5104, 1
Terrell, J., & Olsen, K. H. 1970, ApJ, 161, 399
Trap, G., Falanga, M., Goldwurm, A., et al. 2009, A&A, 504, 501
van der Klis, M. 1989, in Timing Neutron Stars: Proc. NATO Advanced Study Institute on Timing Neutron Stars, held April 4–15, 1988, in Çesme, Izmir, Turkey, ed. H. Ögelman & E. P. J. van den Heuvel (New York: Kluwer Academic), 27
van Paradijs, J. 1979, ApJ, 234, 609
van Paradijs, J., Dotani, T., Tanaka, Y., & Tsuru, T. 1990, PASJ, 42, 633
Verner, D. A., Ferland, G. J., Korista, K. T., & Yakovlev, D. G. 1996, ApJ, 465, 487
Waki, I., Inoue, H., Koyama, K., et al. 1984, PASJ, 36, 819
Weinberg, N. N., Bildsten, L., & Schatz, H. 2006, ApJ, 639, 1018
Wijnands, R., in't Zand, J. J. M., Rupen, M., et al. 2006, A&A, 449, 1117
Wijnands, R., Klien Wolt, M., Kuulkers, E., et al. 2007, ATel, 1006
Wijnands, R., Maccarone, T., Miller-Jones, J., et al. 2005, ATel, 512
Wilms, J., Allen, A., & McCray, R. 2000, ApJ, 542, 914
Worpel, H., Galloway, D. K., & Price, D. J. 2013, ApJ, 772, 94
Zhang, W., Jahoda, K., Swank, J. H., Morgan, E. H., & Giles, A. B. 1995, ApJ, 449, 930